RSC Advances

PAPER

View Article Online
View Journal | View Issue

Cite this: *RSC Adv.*, 2024, **14**, 20923

MOFabric: an effective and wearable protective garment towards CWA detoxification†

Selva Balasubramanian,[ab] Arockia Jayalatha Kulandaisamy,[b] Apurba Das[c] and John Bosco Balaguru Rayappan *[ab]

Received 24th May 2024
Accepted 19th June 2024

DOI: 10.1039/d4ra03830d

rsc.li/rsc-advances

In current trends, an imminent development of self-detoxification filters is highly desirable against exposure to chemical warfare agents (CWAs). Exploiting protective materials that can be applicable in day-to-day life for instantaneous detoxification will be of immense importance. The available technologies in the current scenario are susceptible to secondary emission and pose a need for an alternate design strategy for effective degradation. In addition, the choice of active material and successful impregnation on a suitable substrate for developing potential barriers requires complex material design. In this context, the developed self-standing UiO-66 and UiO-66-NH_2 functionalized fabrics (MOFabrics) present an expeditious detoxification performance against CWA simulant, methyl-paraoxon, with a maximum removal percent conversion of 88.9 and 90.68%. It shows a reduced half-life of approximately 10.16 and 11.23 min, in comparison to an unmodified/carboxymethylated fabric of 462 min.

1 Introduction

To achieve the basic level of self-defense in the materialized era, ideal barriers to protect civilians from accidental or deliberate emissions of chemical warfare agents (CWAs)[1,2] must be developed.[3] The current protective systems widely contain activated carbon as an effective adsorbent due to advantageous properties namely hydrophobicity, easy shaping, and high porosity.[4,5] Nevertheless, the extent of their utilization has been circumscribed due to their secondary emission, heaviness, and lack of selective adsorption.[6,7] To overcome these limitations, the development of self-detoxifying materials is highly desired not only to capture but also to detoxify noxious agents instantaneously to safeguard individuals in toxic zones.[8] To implement this task, zirconium-based metal–organic frameworks (MOFs), such as UiO-66,[9] UiO-66-NH_2,[10] UiO-67,[11] MOF-808,[12] and NU-1000,[13] have gained research interest due to their expeditious catalytic degradation performance. It is ascribed to the presence of many Lewis-acidic Zr^{IV} nodes[14,15] that can effectively catalyze the organophosphorus hydrolysis,[16,17] which is an active ingredient of nerve agents. For instance, the catalytic performance of the aforementioned MOFs has superior detoxification performance against the real nerve agent, 'Soman' (GD), and simulant, 'methyl paraoxon' (DMNP), which have small half-life times of 3.5 and 1 min, respectively.[10,18,19] Besides, the reactivity of MOFs with CWAs is quite slower through a solid-phase decontamination pathway than in an aqueous medium, which resembles the prerequisite of buffer for an effective catalytic performance.[20]

Although MOFs act as a potential candidate for detoxification *via* effective catalytic action,[21] their existence in isolated powder form is impractical in real-time scenarios for large-scale production. Such micro-/nanoparticles might aggregate in the environment or natural ecosystems during the detoxification process and it is implausible to recover the adsorbents again.[22] Hence, it is highly desirable to hybridize such catalytically active MOFs with protective modules, such as cartridge filters,[23] self-standing polymeric membranes,[24,25] packed column beads,[26] and wearable garments with applications as an effective real-time filtration entity.[27] Among these, the development of catalytically active MOF-impregnated fabrics, in combination with air permeability, gives rise to the self-detoxifying filtration fabric.[27] In addition, to make it viable in a practical environment, surface modification with better adherence and more surface coverage area is to be considered are key metrics for designing protective clothing.[28] We must ensure the uniform adherence of MOF particles on the cotton fabrics and eliminate the aggregation and detachment of MOF from the surface. Hence, enhancing the covalent interaction between the MOF and fabric would be a desirable approach rather than physical adhesion.[29]

To date, a plethora of methods, such as atomic layer deposition (ALD),[30] physical spraying,[31,32] layer-by-layer assembly (LBL),[33,34] electrospinning,[35,36] contra-diffusion,[37] microwave

[a]*Centre for Nanotechnology & Advanced Biomaterials (CeNTAB), SASTRA Deemed University, Thanjavur, Tamil Nadu – 613 401, India. E-mail: rjbosco@ece.sastra.edu; Fax: +91 4362 264 120; Tel: +91 4362 350 009 ext: 2255*

[b]*School of Electrical & Electronics Engineering (SEEE), SASTRA Deemed University, Thanjavur, Tamil Nadu – 613 401, India*

[c]*Department of Textile & Fibre Engineering, Indian Institute of Technology Delhi, Hauz Khas, New Delhi – 110 016, India*

† Electronic supplementary information (ESI) available. See DOI: https://doi.org/10.1039/d4ra03830d

irradiation,[38] and polymer functionalization,[39,40] have been employed for the impregnation of MOFs on various substrates. However, surface modification with these approaches continues to pose substantial challenges, likely complexity, in the fabrication process, such as limited MOF loading, long processing time, requirement of elevated temperature, and scale-up limitability. In addition, the surface modification of cotton fabrics is quite challenging due to numerous hydroxyl groups conjoined through hydrogen bonds, which hinder the adhesion of MOFs to their surface.[41] Herein, a facile deposition of UiO-66 and UiO-66-NH_2 MOFs on cotton fabrics by solvothermal method has been demonstrated at low temperatures. Prior to the deposition of MOFs, a two-step pretreatment process namely scouring and carboxymethylation was adopted. These processes enable an increase in the free hydroxyl groups by breaking the hydrogen bonds to a large extent[41] and enhancing MOF nucleation over the surface. The *in situ* growth of MOFs on the cotton surface was studied with respect to its deposition conditions. The catalytic degradation potential of MOF-modified cotton fabrics, "MOFabrics", has been tested against DMNP at room temperature. The extent of degradation performance of MOF-loaded fabrics and isolated MOF crystal powders was analyzed.

2 Materials & methods

2.1 Chemicals

Zirconium(iv) chloride ($ZrCl_4$, CAS No.: 10026-11-6) and 2-aminoterephthalic acid (NH_2-H_2BDC, CAS No.: 10312-55-7) were purchased from TCI Chemicals, Japan. Terephthalic acid (H_2BDC, CAS No.: 100-21-0), Triton X - 100 (CAS No.: 9036-19-5), paraoxon – methyl (DMNP, CAS No.: 950-35-6), and 4-ethylmorpholine (*N*-EM, CAS No.: 100-74-3) were purchased from Sigma-Aldrich, USA. *N*,*N*-Dimethylformamide (Dry DMF, CAS No: 68-12-2) was purchased from Avra Synthesis, India. Isopropyl alcohol (IPA, CAS No.: 67-63-0) was supplied by Pure Chemicals, India. Sodium hydroxide pellets (NaOH, CAS No.: 1310-73-2) were purchased from Sisco Research Laboratories, India. Acetic acid (AA, Glacial extra pure, CAS No.: 64-19-7) was purchased from CDH Fine Chemical, India. Sodium monochloroacetate (SMCA, CAS No.: 3926-62-3) was purchased from LOBA CHEMIE Pvt. Ltd, India. Hydrochloric acid (HCl, 37%, EMPLURA®, CAS No.: 7647-01-0) was purchased from MERCK, India. Untreated woven cotton fabrics were supplied by the Department of Textile and Fibre Engineering, Indian Institute of Technology Delhi (IITD), India.

2.2 Pretreatment of cotton fabrics

2.2.1 Scouring. According to literature,[42] grease, wax, and other additive chemicals on the cotton fabric were removed by immersing the cotton swatches (4×4 cm^2) in a scouring solution containing 10 g of NaOH, 1.5 g of AA, and 3 g of Triton X-100 in 1000 mL of deionized (DI) water. The temperature of the solution was maintained at 100 °C for 1 h. Subsequently, the cotton swatches were rinsed with DI water multiple times and finally dried at room temperature. Likewise, four such samples were pretreated for this study.

2.2.2 Carboxymethylation. The carboxymethylation process[43] was carried out to render the surface of the fabric more anionic for better MOF anchoring. The scoured cotton swatches were immersed in 400 mL of IPA; 40 mL of 25% (w/v) NaOH was added to it drop-wise under continuous stirring for 1 h. Subsequently, the solution was kept at 45 °C, and 24 g of SMCA was added to it and continuously stirred for another 3 h. The cotton swatches were then removed from the solution and cured for 30 min at 85 °C, followed by washing thoroughly with DI water and drying in air. Finally, the treated cotton swatches were dipped into 0.8 mL of AA in 400 mL of DI water for 5 min to finish the anionization process. Finally, the carboxymethylated (CMC) modified cotton swatches were washed with DI water and dried at room temperature.

2.3 Deposition of UiO-66/UiO-66-NH_2 on cotton fabrics using a solvothermal method

Two batches of the metal precursor of $ZrCl_4$ (6 mmol) were dissolved in DMF in a borosilicate reagent bottle with the subsequent addition of 8 equi. HCl under constant stirring for 20 min. The contents were then subjected to sonication for 20 min. The solution was left overnight with the addition of pretreated CMC fabric. The two corresponding ligands, H_2BDC (6 mmol) for UiO-66 and NH_2-H_2BDC (8.4 mmol) for UiO-66-NH_2, were then separately prepared by dissolving them in DMF at room temperature. Among them, the solution containing H_2BDC for UiO-66 synthesis and NH_2-H_2BDC for UiO-66-NH_2 were added to the 1st and 2nd reagent bottles containing metal precursor-CMC fabric solution. The solutions were tightly capped and placed in a hot air oven at 80 °C. After 24 h, the reaction was completed, and the solution was allowed to cool down to room temperature. The cotton swatches and the leftover MOF powder samples were washed with DMF (3×) and DI water (3×). Finally, the samples were dried at 80 °C for 24 h under vacuum (600 mmHg). The deposition methodology is represented in Fig. 1.

2.4 Catalytic hydrolysis of DMNP

For the catalytic experiment, 6.7 mg of each as-prepared MOF (UiO-66 & UiO-66-NH_2) powder catalysts were added separately in an Eppendorf tube containing an aqueous solution of *N*-EM buffer solution (0.45 M). The resultant suspension was stirred for 20 min to obtain a homogeneous reaction mixture. To the reaction mixture, 0.025 mmol of DMNP was added, and 10 μL of aliquot was taken out over certain time intervals (0.5 to 180 min) and diluted with 5 mL of *N*-EM solution. The DMNP degradation was evaluated by monitoring the formation of 4-nitrophenolate/*p*-nitrophenoxide (4-NP), whose absorbance peak was observed at 403 nm. The abovementioned DMNP degradation procedure was executed by replacing the powder samples with 67 mg of MOFabric samples.

2.5 Characterization techniques

Powder X-ray diffraction (PXRD) patterns of MOFabric samples were recorded by Bruker D8 Focus X-ray diffractometer of 2θ

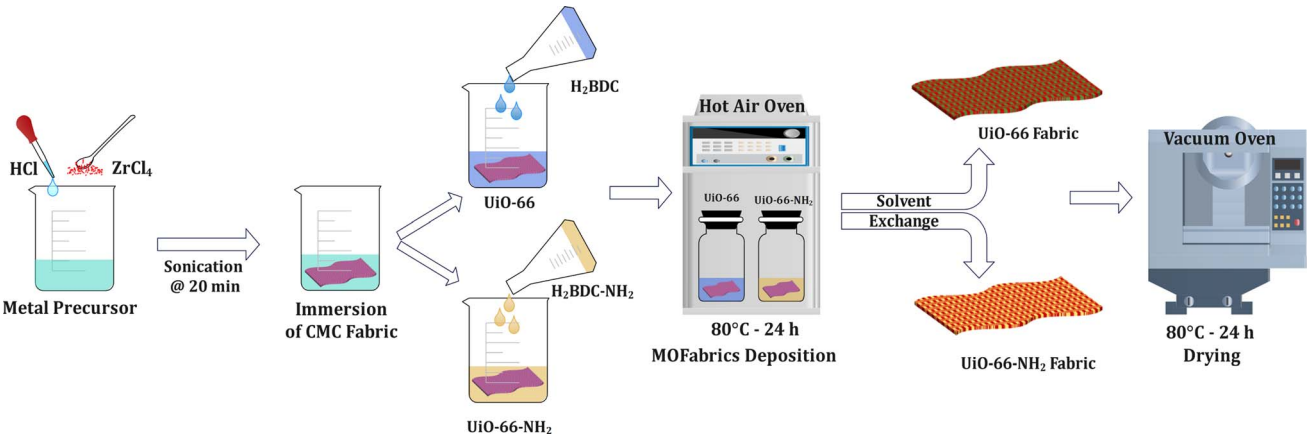

Fig. 1 Solvothermal method to deposit UiO-66 and UiO-66-NH_2 MOFs on cotton fabrics.

ranges between 5 and 40° with a step size of 0.01 degree per sec. SEM imaging was done using VEGA TESCAN, and elemental mapping data was acquired from Zeiss SmartEDX. The chemical composition data was estimated using an X-ray photoelectron spectrometer (XPS, K-ALPHA, Thermo Scientific). Functional group analysis was carried out in transmission mode using a Bruker Alpha-T Fourier Transform Infrared (FTIR) spectrometer. Thermogravimetric Analysis (TGA) was performed to analyze its thermal stability by estimating its weight loss using TA instruments. The catalytic degradation reaction was monitored using a Thermo Scientific Evolution 201 UV-vis spectrophotometer.

3 Results & discussion

3.1 PXRD analysis

The immobilization of UiO-66 and UiO-66-NH_2 MOFs on the CMC fabric was confirmed from the predominant characterization peak (1 1 1) observed at 7.2°. This is in line with the PXRD patterns of powder samples as shown in Fig. 2(a) and (b). Another characteristic peak of the (0 0 2) plane at around 8° with minimal intensity confirmed the successful coating of isoreticular UiO-66 and UiO-66-NH_2. However, the remaining characteristic peaks of MOFabrics at higher angles mainly arise from the CMC functionalization. The superposition of CMC diffraction peaks over the MOF-modified fabrics revealed the unaltered crystallinity of the substrate. As shown in Fig. 2(a) and (b), the CMC fabric has characteristic peaks at 6.2, 7.6, 12.2, and 20.4°. On the other hand, the precipitated MOF powder crystals of UiO-66 and UiO-66-NH_2 exhibit a stronger crystallographic pattern than MOF-anchored CMC fabrics. These patterns match with a crystallographic database (Card No. 4512072).[44,45]

3.2 Morphological studies

In Fig. 3, the change in the color of fabrics to smoked white and yellow from milky white revealed the growth of UiO-66 and UiO-66-NH_2 MOF particles on the surface of cotton fabrics. SEM micrographs of the MOFabrics confirmed the successful impregnation of MOFs over cotton fabrics. During solvothermal deposition, the metal ions in precursor solutions create bonds with carboxylate anions of the CMC fabric, followed by the linkage with organic ligands resulting in the growth of MOF crystals on the fabrics' surface[46] called MOFabrics. It can be seen from the micrographs of MOFabrics (Fig. 3(e) and (f)),

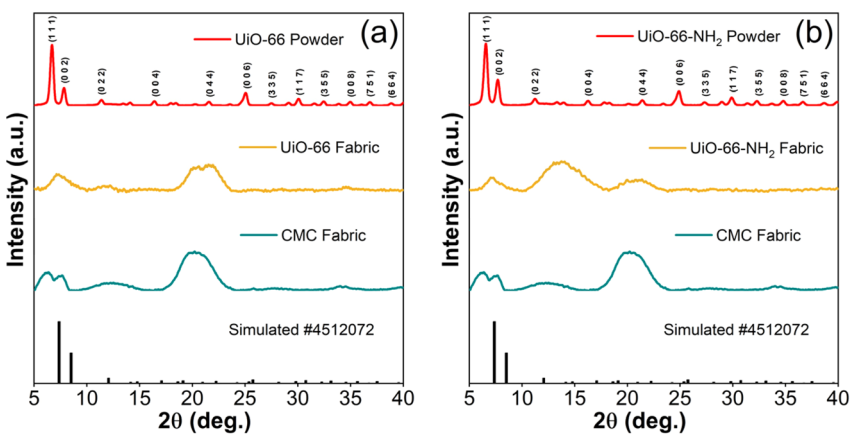

Fig. 2 PXRD patterns of (a) CMC fabric, UiO-66 fabric & powder, and (b) CMC fabric, UiO-66-NH_2 fabric & powder.

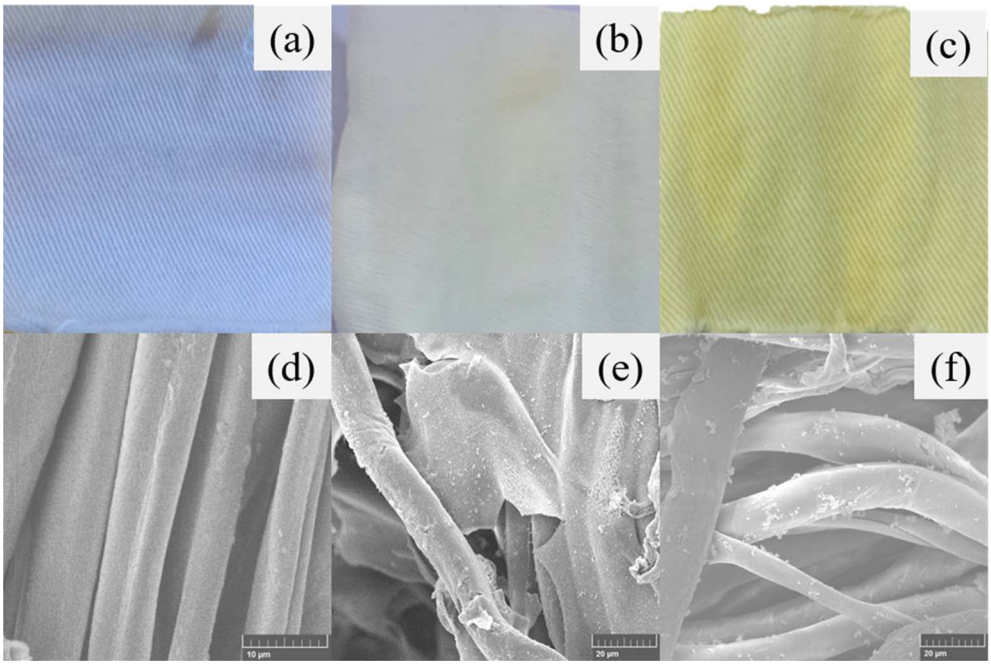

Fig. 3 Photographic and SEM images: ((a) and (d)) CMC fabric, ((b) and (e)) UiO-66 fabric, and ((c) and (f)) UiO-66-NH_2 fabric.

where the UiO-66 and UiO-66-NH_2 MOF particles are formed over the fibers of fabrics in comparison with CMC fabric (Fig. 3(d)). The modified MOF fabric retains its texture and durability, and the disintegration of MOFs from fabrics was not noticed in the course of the experimental procedure. The surface coverage of the as-grown MOFs on the CMC fabrics and the powdered samples were investigated and validated using elemental mapping, as shown in Fig. S1 and S2.† In addition, the SEM micrographs corresponding to the powder form of both, UiO-66 and UiO-66-NH_2, exhibited irregular spheroidal-like structures, which is in line with existing reports.[47,48] The elemental mapping confirmed the uniform distribution of relative elements (Zr, C, O, and N) over the entire surface of MOFabrics, as well as the isolated powder samples. From the quantitative analysis of elemental mapping, the average atomic percentage of each element was estimated and is depicted in Table S1.†

3.3 XPS analysis

To determine the chemical composition of as-prepared MOF samples and their interaction with the CMC cotton fabrics, XPS analysis was performed. The survey spectra confirmed the existence of Zr, C, and O for UiO-66 samples (powder & fabric) and Zr, C, O, and N for UiO-66-NH_2 samples (powder & fabric); they are depicted in Fig. S3–S6.† The chemical composition of all samples was characterized by deconvoluting their corresponding high-resolution spectra. The change in elemental composition values between powder and fabric samples is depicted as a 3-D histogram in Fig. 4. The high-resolution spectrum of Zr 3d can be deconvoluted into two peaks, namely Zr $3d_{5/2}$ and Zr $3d_{3/2}$ with a binding energy difference of ~2.38 eV[49] and relative intensities with a ratio of 3 : 2 ascribed to Zr^{4+} have confirmed the Zr–O bond formation in metal clusters of a framework. The C 1s spectrum was deconvoluted into three distinct peaks namely C=O, C–O, and C–C for UiO-66 samples, and four peaks for UiO-66-NH_2 samples, corresponding to C=O, C=C, C–N, and C–C.[50] The O 1s spectrum was deconvoluted into COOH, Zr–O–C, and Zr–O–Zr for the UiO-66 samples[51] and COOH, C=O, and Zr–O for the UiO-66-NH_2 samples.[52] These peaks were centered at ~532, ~531, and ~529 eV corresponding to μ_3-OH, Zr-carboxylate, and μ_3-O bonding.[53] The N 1s spectrum was deconvoluted as NH_3^+ and NH_2 for UiO-66-NH_2 samples.[54]

According to the deconvoluted spectra, the peak position of each elemental composition of the isolated powders and MOFabrics has negligible deviation. However, significant changes were observed in the atomic ratio of elemental composition and the corresponding values are listed in Tables S2 and S3.† For instance, the quantification of C–O binding for UiO-66 fabric is 11.96%, whereas for the isolated powder sample, it is 22.68%. On the other hand, the atomic percent corresponding to C–C binding in the UiO-66 fabric sample increased to 74.81% of the isolated powder whose value was 58.91%. However, the prominence of such aliphatic C–C bonding was not observed in UiO-66-NH_2 samples. Herein, the values of C–N binding were higher (33.42%) in the fabric sample rather than in the powder sample (19.45%), which might be due to the augmented interaction of amines with the cotton cellulose substrate.

In addition, an increase in the composition of COOH was observed in the MOFabric samples than their corresponding powders, which was due to the elevated breakage of hydrogen bonds during the scouring and carboxymethylation process. To probe the stability of as-prepared MOF powder and fabric

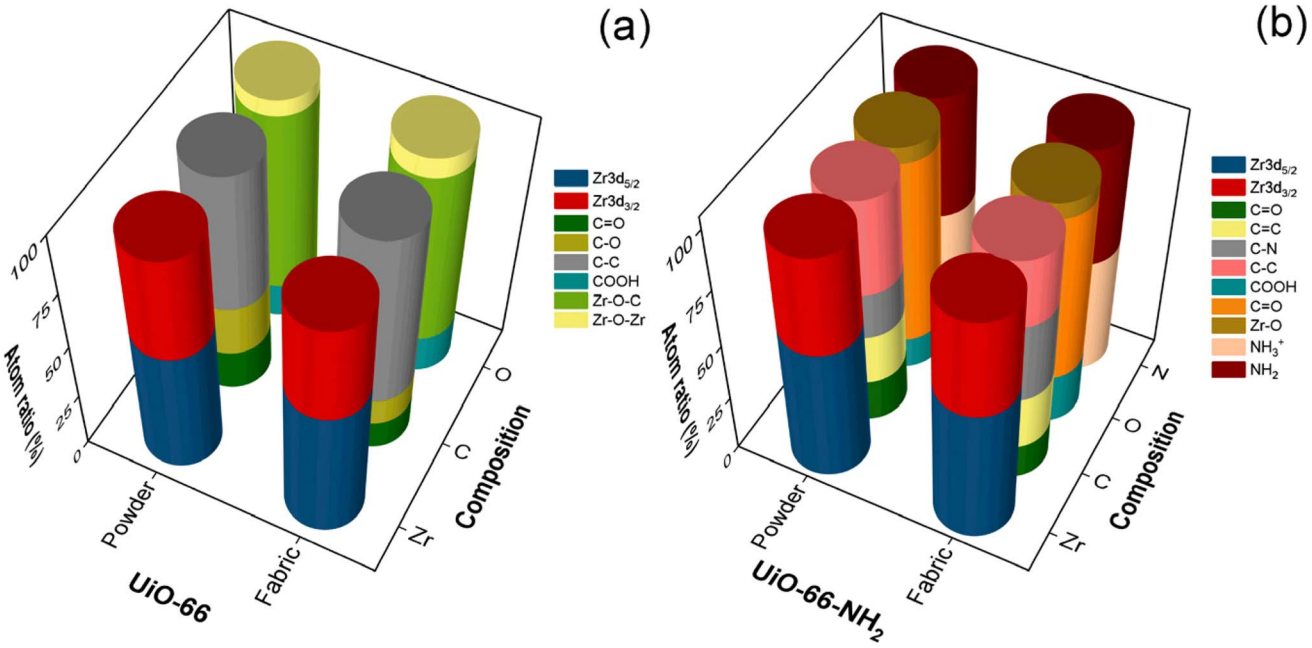

Fig. 4 Chemical composition of MOFs from XPS analysis: (a) UiO-66 (powder & fabric) and (b) UiO-66-NH_2 (powder & fabric).

samples, XPS analysis was done before and after the catalytic degradation of DMNP. From Fig. S7 and S8,† it was found that the binding energy difference between the $3d_{5/2}$ and $3d_{3/2}$ states of Zr remains the same at ~2.38 eV, which corroborated the existence of Zr^{4+} valence state even after multiple catalytic cycles. There was no significant change in the chemical shift and the corresponding relative intensity values. This exceptional stability proves the potency of Zr-based MOFs against noxious agents existing in liquid form.

3.4 Functional group analysis

Fig. 5 shows the FTIR spectra of characteristic absorption bands due to functional group interactions in a framework. For powder samples, the broad peak centered at 3354 cm^{-1} in Fig. 5(a) arises due to O–H stretching caused by the adsorbed water molecules and deprotonated carboxylic acids in the H_2BDC ligand.[55] The peaks of absorption bands at 3451 and 3335 cm^{-1} were observed in Fig. 5(b) due to symmetric and asymmetric stretching of primary amino moieties[56] in UiO-66-NH_2. The band appeared at 2930 cm^{-1} due to C–H stretching. The permanence of Zr^{4+} and –COOH interaction was confirmed from the absorption bands detected at 1661, 1395 and 1659, 1385 cm^{-1}, as shown in Fig. 5(a) and (b), correspondingly. The bands that appeared at 1586, 1506 and 1575, 1502 cm^{-1} correspond to the C=C stretching vibration of the phenyl ring in H_2BDC and NH_2-H_2BDC ligand molecules.[57] The strong absorption band at 1255 cm^{-1} was related to the C–N stretching of amines in UiO-66-NH_2 MOF[58] (Fig. 5(b)). The existence of $Zr_6(OH)_4O_4$ clusters in both the MOF powder samples was confirmed by the symmetric and asymmetric vibration of Zr–O[59] observed at 746, 661 and 767, 660 cm^{-1}.

For the MOFabrics, the aforementioned characteristic absorption bands with minor intensity due to fabric

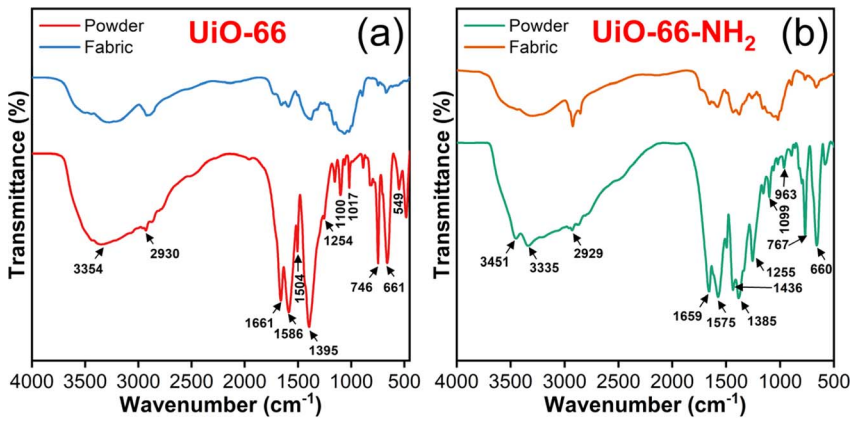

Fig. 5 FTIR spectra of (a) UiO-66 (powder & fabric) and (b) UiO-66-NH_2 (powder & fabric).

dominance. Specifically, the lower intensity of absorption bands 1661, 1395 and 1659, 1385 corresponding to Zr–COOH were ascribed to the crosslinking of anhydride with one side of the fabric and with Zr on the other side. In addition, the adherence of MOFs on the fabric surface might be due to the coordination bond between Zr and the hydroxyl group, which was inferred based on the observed decrease in band intensity around 3300 cm^{-1}. These observations confirm the conformal deposition of MOFs over the CMC fabrics.

3.5 Thermal stability

The TGA aerobic curves of the as-prepared MOF crystals and MOFabrics are shown in Fig. 6. For all the samples, the mass loss that occurred at ~100 °C is due to the removal of water molecules from the pores.[60] The dehydroxylation of $[Zr_6O_4(OH)_4]^{12+}$ to $[Zr_6O_6]^{12+}$ led to weight loss close to around 300 °C.[61] The same process occurred in the MOFabric sample, which underwent a rapid mass loss accompanied by the decomposition of cotton fabric. For the UiO-66-NH_2 MOFabric sample, the mass loss was more intense due to the combustion of NH_2-H_2BDC linker molecules.[62] For UiO-66 samples, the weight loss above 500 °C was due to the complete combustion of H_2BDC linker molecules, leaving behind the residues as ZrO_2. Overall, the UiO-66 MOFabric sample exhibited less residue (17.08%) than the corresponding powder sample (36.67%) due to less thermal stability of fabrics because they can easily combust. A similar trend was observed for the UiO-66-NH_2 samples.

3.6 DMNP hydrolysis

To probe the catalytic efficacy of the MOFabric, the rate of DMNP degradation in the presence of MOFabric samples was estimated by optical pathway.[39] The possible reaction mechanism for such degradation was adopted from literature[63] and has been expressed in Scheme 1. The performance of the MOFabrics in DMNP degradation was assessed by replacing it with CMC fabric and isolated MOF crystals. The degradation kinetics were evaluated from the percent conversion of DMNP to 4-NP over the duration of 180 min, which tracks the absorbance intensity at 403 nm. The degradation curve of DMNP as a function of 4-NP formation *versus* time was plotted as shown in Fig. 7(a) and (b). The concentration of product conversion was estimated from the Lambert–Beer Law, and the initial rate of degradation from the corresponding slope value was obtained. The values of half-life time for all the samples were estimated by presuming that the reaction rate follows the first-order kinetics.[64] The overall conversion efficiency exhibited by the MOFabric samples of UiO-66 and UiO-66-NH_2 were 88.9 and 90.68%. Such conversion is attributed to the presence of Zr^{4+} metal centers in UiO-66 [15] and the synergism of Brønsted base amino moieties,[10] along with Zr^{4+} metal centers in UiO-66-NH_2 MOFs.

The degradation of DMNP is primarily due to the nucleophilic attack at the phosphorus center by strong Lewis acidic Zr^{IV} metal ions that are bridged with a hydroxide group, enabling the cleavage of the phosphorus–oxygen bond. This is because 4-NP is a readily-leaving group, and thus, preferentially generates dimethyl phosphate during the interaction.[20] The phosphate tends to bind either with metal or free hydroxide anions. Finally, the degradation products are dissociated continuously from the reaction sites and catalytic sites are regenerated for a catalytic reaction.[65] The generated byproducts are removed with the aid of *N*-EM buffer, which acts as a base and helps neutralize the acidic products and facilitates the degradation process. In addition, the amino groups in UiO-66-NH_2 samples act as Brønsted bases, enabling easier catalytic activity through the proton transfer process,[66] which enhanced the catalytic performance of resultant MOF/MOFabric samples. The catalytic metrics of MOFabrics were evaluated by comparing its performance in the presence of CMC fabric and without any catalyst (DMNP alone) as shown in Fig. 7(c) and (d). As expected, no significant conversion was observed in this study without a catalyst, and the CMC fabric posed a conversion efficiency of 19% with a half-life of 462 min in a buffered reaction. This might be due to the presence of hydroxyl groups in a cotton fabric. The isolated MOF crystals exhibited a higher removal efficiency of 96.2 and 94.3% for UiO-66-NH_2 and UiO-66 samples, respectively. In comparison to MOF crystals' free powder form, the lessened activity of MOFabric samples was

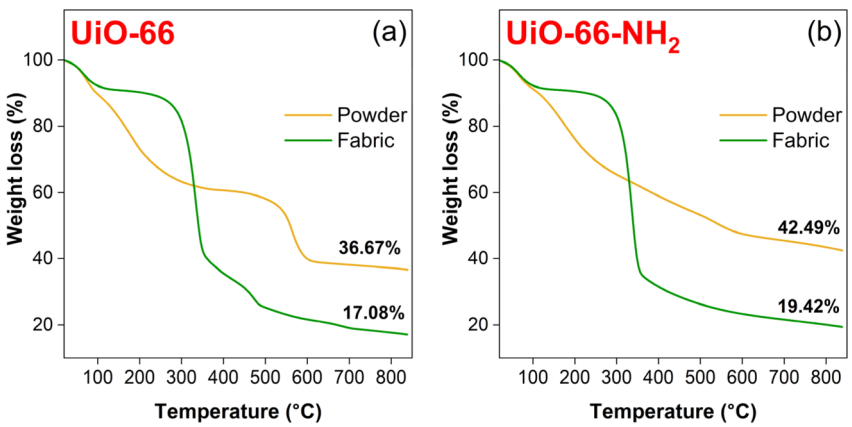

Fig. 6 TGA aerobic curves: (a) UiO-66 (powder & fabric) and (b) UiO-66-NH_2 (powder & fabric) samples.

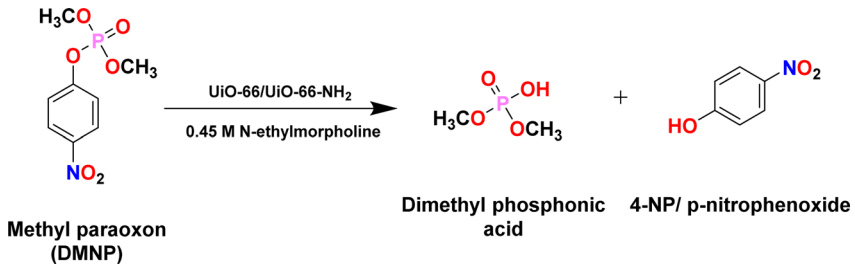

Scheme 1 Catalytic degradation of DMNP using MOF catalyst.

due to the clustering of MOFs on the cotton matrix. However, the deviation in performance levels of isolated powders and MOFabrics was observed to be meagre. The removal efficiency, degradation rate, and half-life time of the different MOF samples are listed in Table 1.

For practical applications, instantaneous hydrolysis was the parameter needed to achieve effective protection from CWAs. In such a scenario, the standalone MOFabric samples exhibited a reduced half-life time of 10.16 (UiO-66) and 11.23 min (UiO-66-NH_2) of DMNP, which was quicker than the contemporary reports.[67] On the other hand, the free form of MOF crystals, UiO-66 and UiO-66-NH_2, exhibited nearly 30 and 26-fold enhancement in reducing the half-life of DMNP than the MOFabrics. This observation that isolated MOF powder has a greater reaction rate and minimal half-life than the functionalized forms of fabrics is in line with existing studies.[68] The usage of the detoxifying agent in the crystal form cannot be realized without the substrate. Hence, the MOFabrics would be a suitable candidate for practical implication, although their performance was slightly lesser than the corresponding crystals. Henceforth, MOFabric samples with a DMNP degradation efficiency of 90.68% proved to be a potential protective clothing moiety against CWAs. However, the improvement of removal efficiency with a shorter degradation time is still desirable to promise the development of self-detoxifying protective garments.

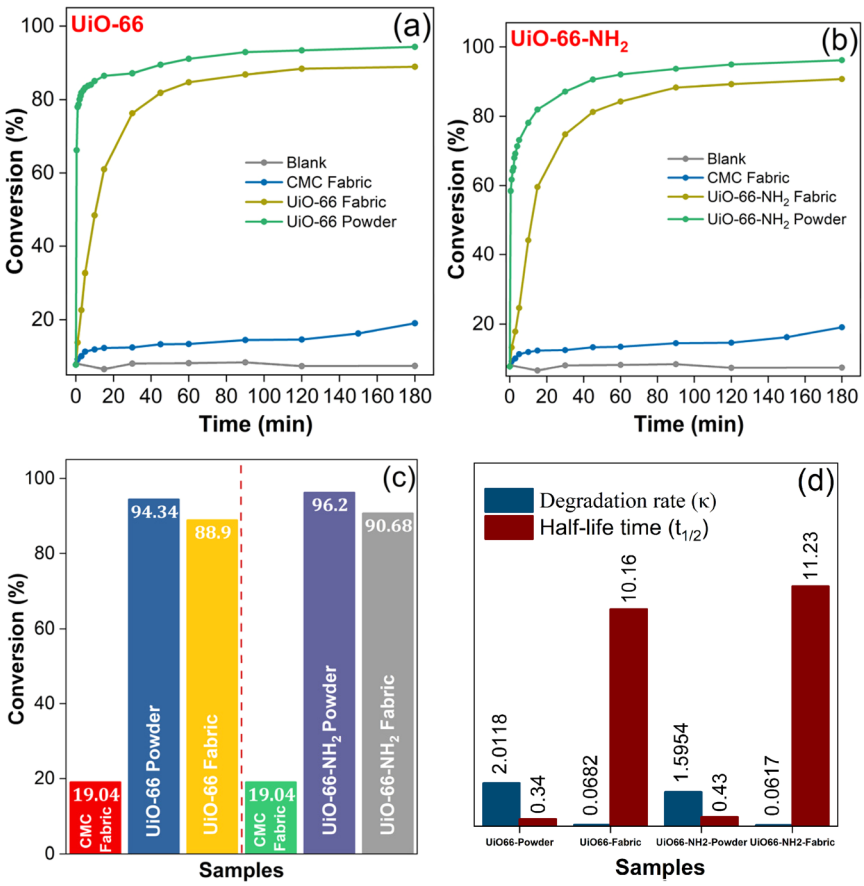

Fig. 7 Catalytic degradation of DMNP to 4-NP as a function of time: (a) UiO-66 (powder & fabric) and (b) UiO-66-NH_2 (powder & fabric), (c) conversion efficiency, and (d) estimated initial rate & half-life.

Table 1 Estimated conversion efficiency, reaction rate, and half-life time of the MOF samples

Sample description		Degradation rate, k (min^{-1})	Half-life (min)	Conversion efficiency (%)
UiO-66	Powder	2.01	0.34	94.34
	Fabric	0.06	10.16	88.9
UiO-66-NH_2	Powder	1.59	0.43	96.2
	Fabric	0.06	11.23	90.68

4 Conclusion

In summary, the current study describes a solvothermal growth protocol for the effective insertion of UiO-66 and UiO-66-NH_2 MOFs into CMC fabrics to achieve protective clothing against DMNP. The developed MOFabrics confirm that the *in situ* surface modification technique allows the formation of MOF hybrid cotton cellulose by enabling chemical interactions between MOF catalysts and fabrics. The combination of UiO-66 and UiO-66-NH_2-loaded fabrics boosted their catalytic activity for the removal of targeted DMNP with a maximum conversion efficiency of 88.9 and 90.68%, respectively. Considering this effectiveness, the present work creates the prospect of developing multifunctional protective defensive garments for real-time scenarios. From the obtained results, we conclude that the modified fabrics can act as a protective suit against real CWAs. Extending the research to meet the essential prerequisites of self-detoxifying garments, such as air permeability, breathability, reusability, and comfort, will facilitate us to materialize an optimized protective suit.

Data availability

Data will be made available on request.

Author contributions

Selva Balasubramanian: methodology, data curation, and writing – original draft preparation. Arockia Jayalatha Kulandaisamy: formal analysis, writing – reviewing and editing. Apurba Das: resources and formal analysis. John Bosco Balaguru Rayappan: conceptualization, writing – reviewing and editing, supervision, project administration, and funding acquisition.

Conflicts of interest

The authors declare no conflict of financial interests.

Acknowledgements

The authors would like to acknowledge the Department of Science and Technology (DST), New Delhi, India (SR/FST/ET-I/2018/221 (C)), and CUB–CSR "Clean Energy and Air" project, India for the funding support. One of the authors, Mr Selva Balasubramanian thanks the Council of Scientific and Industrial Research (CSIR), New Delhi, for providing him a Senior Research Fellowship (09/1095(0058)/2020 EMR-I). We wish to extend our sincere thanks to SASTRA Deemed University, Thanjavur, for providing the infrastructure to carry out this work.

References

1 M. Schwenk, *Toxicol. Lett.*, 2018, **293**, 253–263.
2 M. Zhang, M. Feng, X. Li, Q.-Y. Wang and Q. Ma, *TrAC, Trends Anal. Chem.*, 2024, **172**, 117558.
3 H. L. Schreuder-Gibson, Q. Truong, J. E. Walker, J. R. Owens, J. D. Wander and W. E. Jones, *MRS Bull.*, 2003, **28**, 574–578.
4 J. Przepiórski, in *Activated Carbon Surfaces in Environmental Remediation*, ed. T. J. Bandosz, Elsevier, 2006, vol. 7, pp. 421–474.
5 P. Lodewyckx, in *Activated Carbon Surfaces in Environmental Remediation*, ed. T. J. Bandosz, Elsevier, 2006, vol. 7, pp. 475–528.
6 J. B. DeCoste and G. W. Peterson, *Chem. Rev.*, 2014, **114**, 5695–5727.
7 T. Islamoglu, Z. Chen, M. C. Wasson, C. T. Buru, K. O. Kirlikovali, U. Afrin, M. R. Mian and O. K. Farha, *Chem. Rev.*, 2020, **120**, 8130.
8 B. Picard, I. Chataigner, J. Maddaluno and J. Legros, *Org. Biomol. Chem.*, 2019, **17**, 6528–6537.
9 J. Demel, K. Lang and D. Bůžek, *Inorg. Chem.*, 2018, **57**, 14290–14297.
10 M. J. Katz, S.-Y. Moon, J. E. Mondloch, M. H. Beyzavi, C. J. Stephenson, J. T. Hupp and O. K. Farha, *Chem. Sci.*, 2015, **6**, 2286–2291.
11 X. Lian and B. Yan, *ACS Appl. Mater. Interfaces*, 2018, **10**, 14869–14876.
12 H.-B. Luo, A. J. Castro, M. C. Wasson, W. Flores, O. K. Farha and Y. Liu, *ACS Catal.*, 2021, **11**, 1424–1429.
13 M. C. De Koning, M. Van Grol and T. Breijaert, *Inorg. Chem.*, 2017, **56**, 11804–11809.
14 S. Yuan, J.-S. Qin, C. T. Lollar and H.-C. Zhou, *ACS Cent. Sci.*, 2018, **4**, 440–450.
15 L. Valenzano, B. Civalleri, S. Chavan, S. Bordiga, M. H. Nilsen, S. Jakobsen, K. P. Lillerud and C. Lamberti, *Chem. Mater.*, 2011, **23**, 1700–1718.
16 S. Jang, D. Ka, H. Jung, M.-K. Kim, H. Jung and Y. Jin, *Materials*, 2020, **13**, 2954.
17 S. Pan, X. Nie, X. Guo, H. Hu, B. Liu and Y. Zhang, *Chin. Chem. Lett.*, 2023, **34**, 107620.

18 G. W. Peterson, S.-Y. Moon, G. W. Wagner, M. G. Hall, J. B. DeCoste, J. T. Hupp and O. K. Farha, *Inorg. Chem.*, 2015, **54**, 9684–9686.
19 S.-Y. Moon, G. Wagner, J. Mondloch, G. Peterson, J. DeCoste, J. Hupp and O. Farha, *Inorg. Chem.*, 2015, **54**, 10829–10833.
20 H. Wang, J. J. Mahle, T. M. Tovar, G. W. Peterson, M. G. Hall, J. B. DeCoste, J. H. Buchanan and C. J. Karwacki, *ACS Appl. Mater. Interfaces*, 2019, **11**, 21109–21116.
21 K. Ma, Y. H. Cheung, K. O. Kirlikovali, X. Wang, T. Islamoglu, J. H. Xin and O. K. Farha, *Acc. Mater. Res.*, 2023, **4**, 168–179.
22 A. D. Pournara, E. Moisiadis, V. Gouma, M. J. Manos and D. L. Giokas, *J. Environ. Chem. Eng.*, 2022, **10**, 107705.
23 Z. Gu, W. Song, Z. Yang and R. Zhou, *Phys. Chem. Chem. Phys.*, 2018, **20**, 30384–30391.
24 H.-B. Luo, F.-R. Lin, Z.-Y. Liu, Y.-R. Kong, K. B. Idrees, Y. Liu, Y. Zou, O. K. Farha and X.-M. Ren, *ACS Appl. Mater. Interfaces*, 2023, **15**, 2933–2939.
25 Y.-S. Xie, Y. Peng, Z.-Z. Deng, Z. Zhu, Y. Cheng, D.-H. Ma, L.-Y. Zhu and X.-H. Zhang, *Rare Met.*, 2023, **42**, 4189–4200.
26 K. Kiaei, M. T. Nord, N.-C. Chiu and K. C. Stylianou, *ACS Appl. Mater. Interfaces*, 2022, **14**, 19747–19755.
27 Z. Chen, K. Ma, J. J. Mahle, H. Wang, Z. H. Syed, A. Atilgan, Y. Chen, J. H. Xin, T. Islamoglu, G. W. Peterson and O. K. Farha, *J. Am. Chem. Soc.*, 2019, **141**, 20016–20021.
28 *Handbook of Textile and Industrial Dyeing*, M. Clark, Woodhead Publishing, 1st edn, 2011.
29 D. T. Lee, J. Zhao, C. J. Oldham, G. W. Peterson and G. N. Parsons, *ACS Appl. Mater. Interfaces*, 2017, **9**, 44847–44855.
30 D. T. Lee, J. Zhao, G. W. Peterson and G. N. Parsons, *Chem. Mater.*, 2017, **29**, 4894–4903.
31 E. López-Maya, C. Montoro, L. M. Rodríguez-Albelo, S. D. Aznar Cervantes, A. A. Lozano-Pérez, J. L. Cenís, E. Barea and J. A. R. Navarro, *Angew. Chem., Int. Ed.*, 2015, **54**, 6790–6794.
32 C.-Y. Jiang, M. Feng, C.-T. Yu, Z.-B. Bao, S.-L. Zhu and F.-H. Wang, *Rare Met.*, 2023, **42**, 3859–3869.
33 R. Gil-San-Millan, P. Delgado, E. Lopez-Maya, J. D. Martin-Romera, E. Barea and J. A. R. Navarro, *ACS Appl. Mater. Interfaces*, 2021, **13**, 50491–50496.
34 L. Zhang, J. Sun, Y. Zhou, Y. Zhong, Y. Ying, Y. Li, Y. Liu, Z. Zuhra and C. Huang, *J. Mater. Chem. B*, 2017, **5**, 6138–6146.
35 M. Rose, B. Böhringer, M. Jolly, R. Fischer and S. Kaskel, *Adv. Eng. Mater.*, 2011, **13**, 356–360.
36 A. X. Lu and G. W. Peterson, *ACS Appl. Mater. Interfaces*, 2017, **9**, 1–12.
37 Y. Zhou, X.-F. Zhang, J. Yao and H. Wang, *Sep. Purif. Technol.*, 2022, **300**, 121837.
38 N. Couzon, M. Ferreira, S. Duval, A. El-Achari, C. Campagne, T. Loiseau and C. Volkringer, *ACS Appl. Mater. Interfaces*, 2022, **14**, 21497–21508.
39 J. Zhao, D. T. Lee, R. W. Yaga, M. G. Hall, H. F. Barton, I. R. Woodward, C. J. Oldham, H. J. Walls, G. W. Peterson and G. N. Parsons, *Angew. Chem., Int. Ed.*, 2016, **55**, 13224–13228.
40 R. Ramaseshan, S. Sundarrajan, Y. Liu, R. S. Barhate, N. L. Lala and S. Ramakrishna, *Nanotechnology*, 2006, **17**, 2947.
41 M.-K. Kim, S. H. Kim, M. Park, S. G. Ryu and H. Jung, *RSC Adv.*, 2018, **8**, 41633–41638.
42 T. J. Athauda, P. Hari and R. R. Ozer, *ACS Appl. Mater. Interfaces*, 2013, **5**, 6237–6246.
43 M. Schelling, M. Kim, E. Otal and J. Hinestroza, *Bioengineering*, 2018, **5**, 14.
44 J. Winarta, B. Shan, S. M. Mcintyre, L. Ye, C. Wang, J. Liu and B. Mu, *Cryst. Growth Des.*, 2020, **20**, 1347–1362.
45 S. Øien, D. Wragg, H. Reinsch, S. Svelle, S. Bordiga, C. Lamberti and K. P. Lillerud, *Cryst. Growth Des.*, 2014, **14**, 5370–5372.
46 H. S. Jhinjer, A. Singh, S. Bhattacharya, M. Jassal and A. K. Agrawal, *J. Hazard. Mater.*, 2021, **411**, 125056.
47 J. Du, L. Chen, X. Zeng, S. Yu, W. Zhou, L. Tan, L. Dong, C. Zhou and J. Cheng, *ACS Appl. Mater. Interfaces*, 2020, **12**, 28576–28585.
48 M. Ahmadi, S. M. Ayyoubzadeh, F. Ghorbani-Bidkorbeh, S. Shahhosseini, S. Dadashzadeh, E. Asadian, M. Mosayebnia and S. Siavashy, *Heliyon*, 2021, **7**, e06914.
49 Y. Luan, Y. Qi, H. Gao, N. Zheng and G. Wang, *J. Mater. Chem. A*, 2014, **2**, 20588–20596.
50 X. Fang, S. Wu, Y. Wu, W. Yang, Y. Li, J. He, P. Hong, M. Nie, C. Xie, Z. Wu, K. Zhang, L. Kong and J. Liu, *Appl. Surf. Sci.*, 2020, **518**, 146226.
51 Y. Wang, L. Li, P. Dai, L. Yan, L. Cao, X. Gu and X. Zhao, *J. Mater. Chem. A*, 2017, **5**, 22372–22379.
52 M. Ma, J. Zhang, P. Li, Y. Du, J. Gan, J. Yang and L. Zhang, *Microchim. Acta*, 2021, **188**, 186.
53 A. H. Ibrahim, W. A. El-Mehalmey, R. R. Haikal, M. E. A. Safy, M. Amin, H. R. Shatla, S. G. Karakalos and M. H. Alkordi, *Inorg. Chem.*, 2019, **58**, 15078–15087.
54 M. Peñas-Garzón, M. J. Sampaio, Y. L. Wang, J. Bedia, J. J. Rodriguez, C. Belver, C. G. Silva and J. L. Faria, *Sep. Purif. Technol.*, 2022, **286**, 120467.
55 F. Zhang, W. Cheng, Z. Yu, S. Ge, Q. Shao, D. Pan, B. Liu, X. Wang and Z. Guo, *Adv. Compos. Hybrid Mater.*, 2021, **4**, 1330–1342.
56 Q. Liu, G.-L. Zang and Q. Zhao, *Environ. Sci. Pollut. Res.*, 2022, **29**, 76833–76846.
57 C. Chen, D. Chen, S. Xie, H. Quan, X. Luo and L. Guo, *ACS Appl. Mater. Interfaces*, 2017, **9**, 41043–41054.
58 A. Huang, L. Wan and J. Caro, *Mater. Res. Bull.*, 2018, **98**, 308–313.
59 Y. Zhao, D. Wang, W. Wei, L. Cui, C.-W. Cho and G. Wu, *Environ. Sci. Pollut. Res.*, 2021, **28**, 7068–7075.
60 S. Wu, Y. Ge, Y. Wang, X. Chen, F. Li, H. Xuan and X. Li, *Environ. Technol.*, 2018, **39**, 1937–1948.
61 M. Taddei, *Coord. Chem. Rev.*, 2017, **343**, 1–24.
62 J. Zhu, L. Wu, Z. Bu, S. Jie and B.-G. Li, *ACS Omega*, 2019, **4**, 3188–3197.
63 K.-M. Kim, H.-W. Park, G.-S. Shim, S.-W. Jang, H.-J. Kim, G.-S. Chae, S. Shin and J.-H. Lee, *J. Mater. Sci.*, 2020, **55**, 2604–2617.

64 M. Bagheri, M. Y. Masoomi, A. Forneli and H. García, *J. Phys. Chem. C*, 2022, **126**, 683–692.
65 L. Song, T. Zhao, D. Yang, X. Wang, X. Hao, Y. Liu, S. Zhang and Z.-Z. Yu, *J. Hazard. Mater.*, 2020, **393**, 122332.
66 M. Chen, Y. Tu and S. Wu, *Materials*, 2021, **14**, 2419.
67 N. Couzon, P. Hardy, M. Ferreira, N. Hammi, J. Dhainaut, F. Pourpoint, S. Royer, T. Loiseau, C. Campagne and C. Volkringer, *Dalton Trans.*, 2024, **53**, 5784–5787.
68 D. B. Dwyer, D. T. Lee, S. Boyer, W. E. Bernier, G. N. Parsons and W. E. Jones, *ACS Appl. Mater. Interfaces*, 2018, **10**, 25794–25803.